Kütahya Dumlupınar University
Institute of Graduate Studies

Journal of Scientific
Reports-A
E-ISSN: 2687-6167
Number 53, June 2023

RESEARCH ARTICLE

PERFORMANCE ASSESSMENT OF LANDSAT 8 AND SENTINEL-2 SATELLITE IMAGES FOR THE PRODUCTION OF TIME SERIES LAND USE/LAND COVER (LULC) MAPS

Recep Ugur ACAR[1*], Enes ZENGIN[2]

[1*] Kutahya Dumlupinar University, Geological Engineering, Kütahya, Türkiye,
ugur.acar@dpu.edu.tr, ORCID: 0000-0002-0420-6263
[2] Kutahya Dumlupinar University, Urban and Regional Planning, Kutahya, Türkiye
enes.zengin@dpu.edu.tr, ORCID: 0000-0002-5740-7763

Receive Date:02.12.2022 *Accepted Date: 06.04.2023*

ABSTRACT

Land use/Land cover (LULC) maps are essential tools used in various disciplines, including geosciences, urban and regional planning, climate, and agriculture. LULC maps provide a visual representation of the Earth's surface, depicting the different types of land use and land cover in a given area. Land use refers to the human activities that take place on the land, such as agriculture, urban development, and mining, while land cover refers to the physical characteristics of the land, such as forests, grasslands, and wetlands. Researchers can gain insights into environmental trends and patterns, such as deforestation, urbanization, and climate change by analysing changes in LULC over time. While Landsat 8 images have been used to create LULC maps for years, the high-resolution images provided by Sentinel-2 since 2017 have allowed for the creation of highly detailed LULC maps. However, it is still necessary to use Landsat 8 images to produce LULC maps for time-series analyses and future predictions. Unsupervised classification is a method used to create LULC maps using Landsat 8 images, but this study found that the resulting maps differed from those created using Sentinel-2 images, with up to a two-fold difference in the classification of classes such as "Bare Ground," "Built Area," "Crops," and "Trees". Especially when using Landsat data, it is suggested that it would be useful to make evaluations for wider areas/regions as the resolution of Landsat 8 satellite images is limited to 30 meters.

Keywords: *Landsat 8, Land use map, Land cover map, Sentinel-2, Unsupervised classification*

1. INTRODUCTION

The enactment of global endeavours towards climate change mitigation, sustainable development, and preserving ecosystem and biodiversity functions directly in association with the U.N. Sustainable Development Goals in relation with the production of land use/land cover (LULC) change maps on global, national, and regional scales. The need for globally reliable LULC maps has long been a focus, with the promise of improved quantification made possible using remote sensing data from various

sources like Landsat and Sentinel satellites [1–4]. To meet the need in this regard, the maps have been published in recent years with different spatial resolutions for both global or regional use by Esri Land Cover and European Space Agency World Cover [5,6]. These new and up to date LULC maps provide unprecedentedly heightened spatial and accurate mapping details [7]. However, they lack typology customization or monitoring capabilities required for earth science and urban and regional planning applications. The Landsat program, which is another source which can be used to produce LULC maps operated by the United States Geological Survey (USGS) and the National Aeronautics and Space Administration (NASA), provides satellite data with a medium spatial resolution which is 30 meters [8]. Although satellites such as Sentinel-2 are used widely for LULC today, Landsat is also a significant source for monitoring historical changes, especially since it provides publicly available data from 1972. Since the resolution of Landsat is 30 meters, it provides data with lower resolution than satellites such as Sentinel-2. Despite its limitations, Landsat is used by many researchers for different thematic studies like forest monitoring, structure mapping, vegetation health assessment, flood, and drought analysis, as it can be used for preliminary and fast assessments [9–14].

In addition to the maps provided by various organizations, it is also possible to produce LULC maps with unsupervised learning algorithms by using geographic information systems software like ArcGIS or QGIS [15]. The Iterative Self-Organizing (ISO) Cluster classifier is one of the featured algorithms for unsupervised classification applications with its capability to handle very large images. ISO clustering does not require prior knowledge of the classes present in the satellite image. This makes it a useful tool for exploratory analysis and for identifying patterns and structures in the data. It can identify complex structures in the data, such as irregular shapes and clusters of different densities. This makes it useful for satellite image classification, where objects of interest can have varying shapes and sizes. ISO clustering is computationally efficient and can handle large datasets with many variables, making it suitable for analyzing high-resolution satellite imagery. It is also flexible and can be used with different distance metrics and linkage methods, depending on the characteristics of the data being analyzed. Overall, ISO clustering is a powerful tool for satellite image classification that can identify complex structures and patterns in the data, without requiring prior knowledge of the classes present [4,16]. Furthermore, the ISO cluster classifier can take a segmented RGB raster from a third-party application. ISO cluster classifier can both work with Esri-supported raster files and other segmented raster datasets. The multidimensional attribute space is used by the ISO Cluster algorithm to perform an unsupervised classification to identify the properties of the naturally occurring cell/pixel groupings. In this study, LULC maps for 2017 and 2021were produced using Landsat data with 30 meters spatial resolution for Kütahya located in the western part of the Türkiye which was chosen as the study area, by using the unsupervised learning algorithm. ArcGIS Pro software was used to production LULC maps using an unsupervised learning algorithm. In order to assess unsupervised classification algorithm performance of the LULC maps produced for 2017 and 2021, the LULC maps provided by Sentinel-2 with a resolution of 10 meters were used for each time-series. The relevant satellite images were taken from the June data sets of 2017 and 2021 to reach the lowest cloud density values.

JSR A
Journal of Scientific Reports

2. MATERIALS and METHODS

2.1. Study Area

Kütahya is a major settlement, with a population of 578,640 and a surface area of 11,632 km^2, located in the Aegean Region of Türkiye, was chosen as the study area (Figure 1). Kütahya, which is adjacent to Eskişehir, Afyonkarahisar, Uşak, Manisa, Balıkesir, Bursa and Bilecik, is located on 39°16′10.2″N and 29°33′10.8″E central coordinates. Forests, rangelands and crops are the predominant LULC classes in the study area. Forest areas within the study area are in the mountain regions on the Gediz-Altıntaş and Domaniç-Simav lines. Rangelands are spread in regions where forest areas exist throughout the study area. Agricultural areas are mainly concentrated in the Çavdarhisar-Aslanapa-Altıntaş region.

2.2. Sentinel-2 Collection

The LULC maps have been distributed as open sources since 2017 with 10 meters of high spatial resolution using satellite images from Sentinel-2 by the Environmental Systems Research Institute (ESRI). The dataset was classified by applying a high-level of deep learning algorithm that classifies surface reflectance data on Sentinel-2 satellite images [5]. The Sentinel-2 satellite has a multispectral imager that captures images in 13 spectral bands, which are divided into four groups. Among these, six bands are particularly important for monitoring and assessing vegetation health, water quality, and land use/land cover changes. The first band is the coastal aerosol band, which has a wavelength range of 443 nanometers and is used to study the concentration of aerosols and chlorophyll-a in coastal waters. The blue band, with a wavelength range of 490 nanometers, is used to monitor water quality and vegetation health. The green band, with a wavelength range of 560 nanometers, is used to study vegetation health and growth. The red band, with a wavelength range of 665 nanometers, is used to assess vegetation health, identify different crop types, and monitor forest cover. The vegetation red edge band, with a wavelength range of 705 to 745 nanometers, is used to study vegetation health and growth. Finally, the near-infrared band, with a wavelength range of 785 nanometers, is used to monitor vegetation density, water content, and soil moisture. In addition to these six bands, the Sentinel-2 satellite also captures images in the high-resolution visible (HRV) band and six shortwave infrared (SWIR) bands, which are used to study mineral content, soil moisture, and land use/land cover changes. As a result of using different bands with various wavelengths, final LULC maps were produced with nine different classes; water (rivers, ponds, lakes), trees (dense/tall vegetation), flooded vegetation (irrigated and inundated agriculture), crops (corn, wheat, soy), built area (houses, dense villages, cities), bare ground (rocks, soils, mines), snow/ice (glaciers), clouds and rangeland (bushes, shrubs, grass). 10-meter resolution GeoTIFF scenes from 2017 and 2021 were downloaded to create LULC maps for the study area based on Sentinel-2 data which was used to assess the unsupervised classification performance of Landsat 8 data.

JSR A
Journal of Scientific Reports

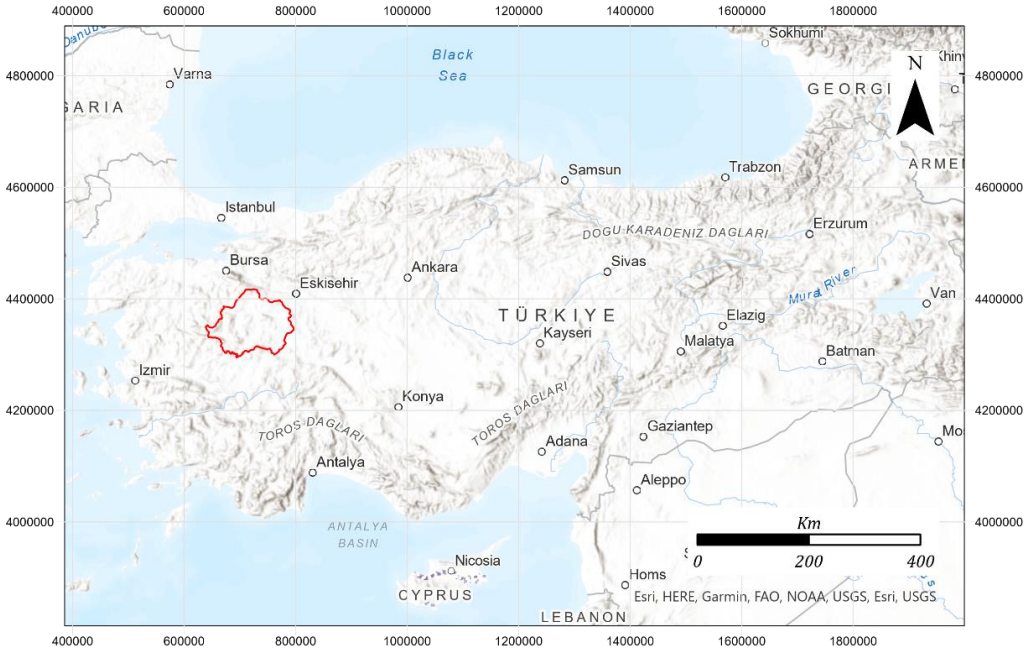

Figure 1. Study area.

2.3. Landsat 8 OLI/TIRS Collection

Traditional digital cameras are designed to imitate as the human eye sees, for this they capture light only in the red, green and blue wavelengths. Then those cameras apply red, green and blue filters to these wavelengths to create a natural RGB image. There will be a lot of information to work on a multispectral image from a complex sensor system like Landsat 8. Different wavelengths would be useful for researchers to discern some features more and better than others or even help to see through features such as clouds or smoke using various bands. Near Infrared (NIR) wavelength is one of the most typically used wavelengths on multispectral sensors because vegetation reflects intensely in this part of the electromagnetic spectrum. In this way, this information provides a handy method for vegetation analysis. The Shortwave Infrared (SWIR) bands on Landsat 8 are very useful for discerning disparities in bare earth and describing what is wet and dry in a study area. There are many other benefits of the available bands in Landsat 8 images that can be used for different purposes. Landsat 8 has two primary sensors, which are the Operational Land Imager (OLI) and Thermal Infrared (TIRS). OLI produces nine spectral bands varying from Band 1 to Band 9 with 15, 30 and 60-meter resolution. Using the OLIs 9 spectral band to discriminate vegetation, biomass, vigour and similar focuses is possible. TIRS of Landsat 8 consists of 2 thermal bands with a spatial resolution of 100 meters and can be used for tracking land and water usage by measuring the Earth's thermal energy. Bandwidths and resolutions of OLI and TIRS sensors of Landsat 8 are given in Table 1 [17]. In order to assess the unsupervised classification performance, Landsat 8 OLI/TIRS Collection 2 Level-2 science product with 30-meter multispectral data belong paths and rows covering (179-32,

179-33, 180-33) the study area were used. The summer periods of 2017 and 2021 were chosen as the acquisition dates to have the least cloud density and more high-quality outputs in classification. For this reason, attention was paid to ensuring that the cloud cover was less than 5% while accessing the Landsat 8 images.

Table 1. Landsat 8 OLI and TIRS bandwidth and resolutions [17].

Band Name	Bandwidth (µm)	Resolution (m)
Band-1: Coastal	0.43 – 0.45	30
Band-2: Blue	0.45 – 0.51	30
Band-3: Green	0.53 – 0.59	30
Band-4: Red	0.64 – 0.67	30
Band-5: NIR	0.85 – 0.88	30
Band-6: SWIR 1	1.57 – 1.65	30
Band-7: SWIR 2	2.11 – 2.29	30
Band-8: Pan	0.50 – 0.68	15
Band-9: Cirrus	1.36 – 1.38	30
Band-10: TIRS 1	10.6 – 11.19	100
Band-11: TIRS 2	11.5 – 12.51	100

The most common band combinations used in this study were summarized to provide helpful information for researchers. The natural colour composite uses a band combination of red (4), green (3), and blue (2), which can be used to detect urban features. These composite replicates what human eyes can see very similarly. Urban features appear white and grey, while water is dark blue or black. It is also possible to distinguish healthy vegetation with green and unhealthy flora with brown colour. The colour-infrared combination is also called the near-infrared (NIR) composite. It uses near-infrared (5), red (4), and green (3). As chlorophyll reflects near-infrared light, NIR band composition is proper for investigating vegetation. In particular, areas in red have better vegetation health, while dark areas are urban areas and water zones. SWIR-1 (6), near-infrared (5), and blue (2) band combination is instrumental in detecting agriculture zones and crop monitoring as this combination uses short-wave and near-infrared, which provide reliable results for vegetation. This band combination shows healthy vegetation with darker shades of green, while the bare surface has a magenta hue. Another band combination that efficiently determines geological elements, lithological features, and faults uses SWIR-2 (7), SWIR-1 (6), and blue (2). Furthermore, other band combinations are needed for extensive geological features like rock types and ore deposit exploration. The bathymetric band combination uses the red (4), green (3), and coastal bands to penetrate the water. The coastal band is good in coastal, bathymetric, and aerosol analyses because it reflects blues and violets. This band combination is good for assessing and evaluating sedimentation in water. The Landsat 8 band combinations and RGB codes used are given in Table 2.[17].

Table 2. Landsat 8 band combinations for different applications [17].

Band Combinations	Red	Green	Blue
Natural Colour	4	3	2
False Colour (Urban)	7	6	4

Colour Infrared (Vegetation)	5	4	3
Agriculture	6	5	2
Atmospheric Penetration	7	6	5
Healthy Vegetation	5	6	2
Land/Water	5	6	4
Shortwave Infrared	7	5	4
Vegetation Analysis	6	5	4

2.4. Processing Flow

The flow given in Figure 2 was applied to create LULC maps using Landsat 8 data with unsupervised classification and to assess the unsupervised classification performance using Sentinel-2 LULC. The study can be divided into three sub-groups data preparation, pre-processing, and evaluation. As a part of the data preparation, Landsat 8 and Sentinel-2 images were combined and cropped into a single mosaic raster covering the study area. To slightly increase the resolution of Landsat 8 images, pixels with a resolution of 30 meters were resampled to 10 meters. The same processes were applied to Sentinel-2 images, except for resampling.

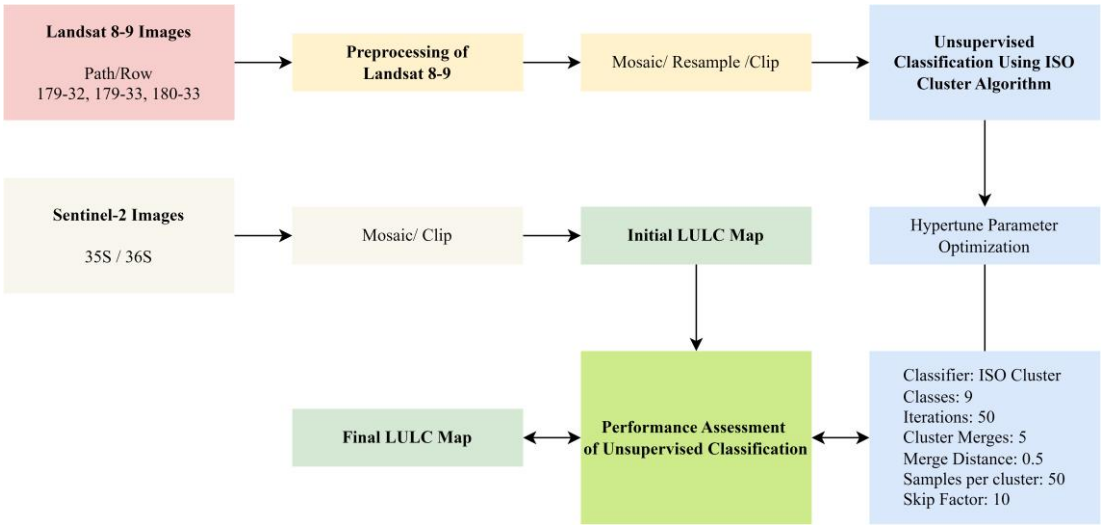

Figure 2. Flowchart for assessing unsupervised classification algorithm performance.

3. UNSUPERVISED CLASSIFICATION PROCESS

Pixel-based classification method was used during the production of the maps with the unsupervised learning algorithm [18]. This classification approach performs on a per-pixel base, where the spectral attributes of the individual pixel determine the class to which it is assigned. Characteristics of adjacent pixels are not considered in the pixel-based technique. Pixel-based classification can be described as a more traditional method and may result in speckled outcomes in the classified image. Another critical

stage of unsupervised learning is to decide the classification schema, which determines the total number of classes in the final raster. Sentinel-2 LULC map classes were used to classify the Landsat 8-based rasters. Several crucial variables impact the outcome images in the categorization procedure using the unsupervised learning algorithm. The ISO Cluster classifier performs an unsupervised classification using the K-means approach [19]. The K-Nearest Neighbour classifier performs a K-nearest neighbour classification, classifying a pixel by a plurality voting of its neighbours. The training process assigns the training samples to their individual classes. K is the defined number of neighbours used in voting. In order to achieve a statistically meaningful signature file generation process for the forthcoming classification, each individual cell should have appropriate cells that represent related clusters accurately. In this study, it was determined the minimum class size is ten times bigger than the number of layers in the input raster bands. The value chosen for the selection interval implies one cell out of every n-by-n block of cells is used in the cluster calculations [19]. Commonly, the additional cells included in the extent of the intersection of the input bands, the more heightened the values for minimum class size should be specified along with the sample interval. However, the sample interval value should be small enough to represent the most diminutive categories in the rasters or input data. It is always possible to achieve better results as long as all input bands have the same data ranges. The data ranges can be transformed to the same range using Map Algebra to perform the equation, as the band have broadly different data ranges [16,20]. The map algebra formula that applied is given in Equation 1 below;

$$Z = \frac{(X - oldmin)\ x\ (newmax - newmin)}{(oldmax - oldmin)} + newmin \tag{1}$$

where;

- *Z:* output raster with new data ranges,
- *X:* input raster, *oldmin* is the minimum value of the input raster,
- *oldmax:* maximum value of the input raster,
- *newmin*: desired minimum value for the output raster,
- *newmax:* desired maximum value for the output raster.

Furthermore, the maximum number of classes must be defined in the output raster. The number of classes in the Sentinel-2 maps used in the analysis of unsupervised classification performance was chosen as the maximum number of classes which is 9. The maximum number of iterations during unsupervised classification is an important parameter. This number defines the maximum number of iterations the clustering process will run. In order to achieve the optimum number of iterations during the processing, 50, 100 and 250 iterations were chosen. As a result of the hyper-tuning parameter technique, 50 was chosen the maximum number of iterations. However, a number between 10 and 20 is suggested to keep the processing time acceptable. All of the hyperparameters preferred during the creation of LULC maps using Landsat 8 images are given in Figure 2.

JSR A
Journal of Scientific Reports

4. RESULTS

LULC maps created for 2017 and 2021 using images provided by Sentinel-2 and available as open source by ESRI are given in Figure 3 and Figure 4. It was decided to assess the unsupervised classification performance based on the LULC maps produced using the satellite images provided by Sentinel-2 as they have 10 meters spatial resolution. Therefore, field classes were separately calculated for the years 2017 and 2021. Class details and the percentage of all individual classes are given in Table 3. According to the LULC maps produced for 2017 and 2021 using Sentinel-2 satellite images, the highest increase was seen in "Crops" at 2.3%, "Trees" at 0.9% and "Built Area" at 0.5%. The change in these classes are 264.2 km^2, 102.2 km^2 and 60.3 km^2, respectively. These three classes constitute 96.3% of the study area. All nine classes in the LULC maps produced by ESRI can be seen in the study area. These data were used to analyze the performance of the unsupervised classification using Landsat 8 images. LULC maps created for 2017 and 2021 by unsupervised learning using Landsat 8 images are given in Figure 5 and Figure 6. All nine classes in Sentinel-2 do not appear on the generated LULC maps. Accurately classifying areas with flooded vegetation, snow/ice, water and clouds was not possible. The main reason for the low performance of unsupervised classification of some field types is that the resolution of Landsat 8 data is limited to 30 meters.

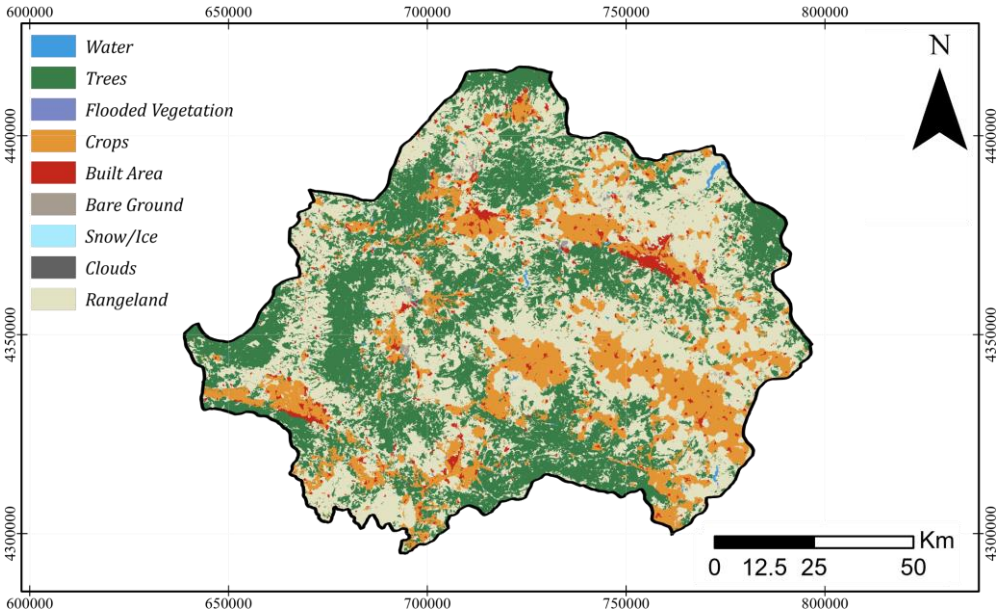

Figure 3. 2021 LULC map produced by using Sentinel-2 satellite images.

JSR A
Journal of Scientific Reports

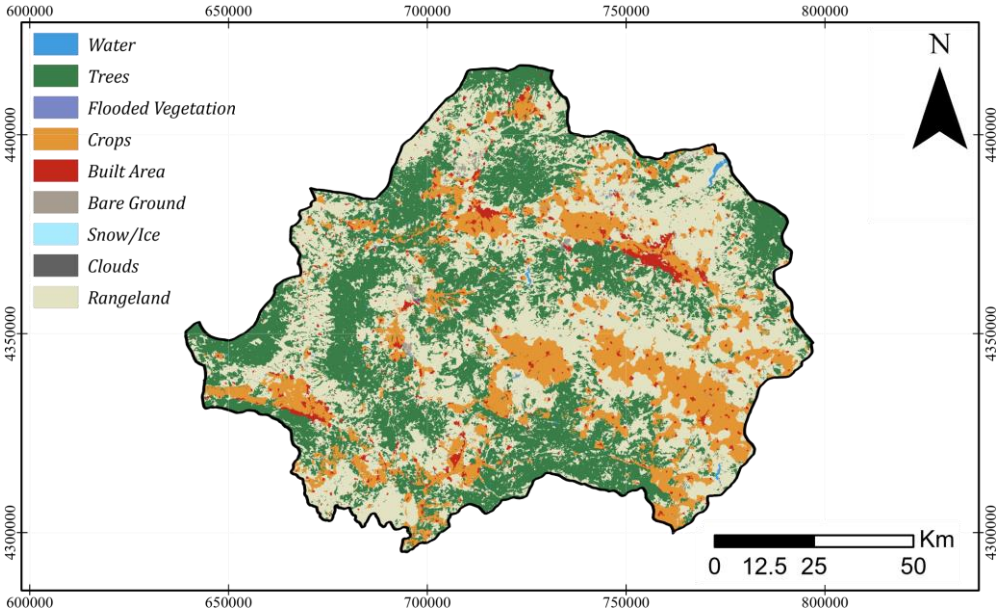

Figure 4. 2017 LULC map produced by using Sentinel-2 satellite images.

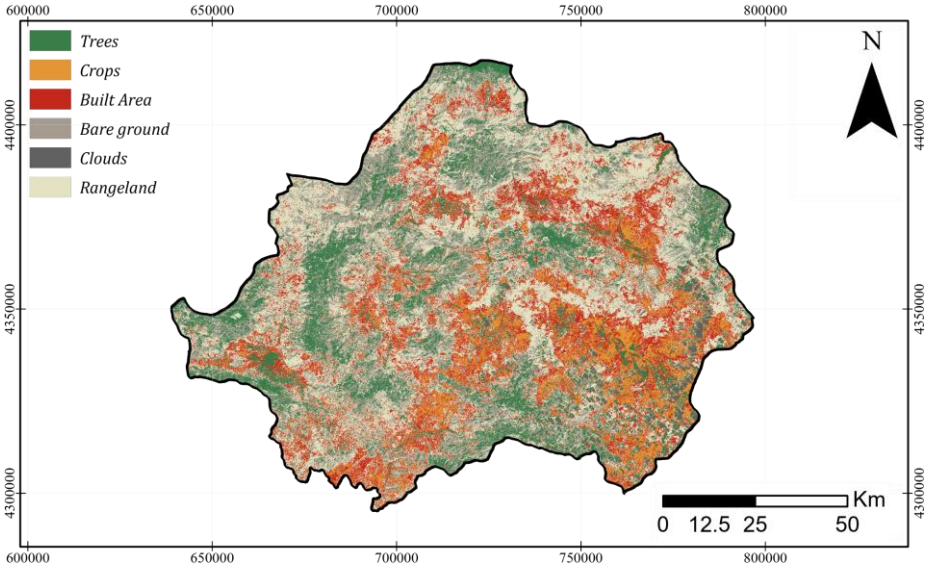

Figure 5. 2021 LULC map produced with unsupervised learning algorithms by using Landsat 8 satellite images.

JSR A
Journal of Scientific Reports

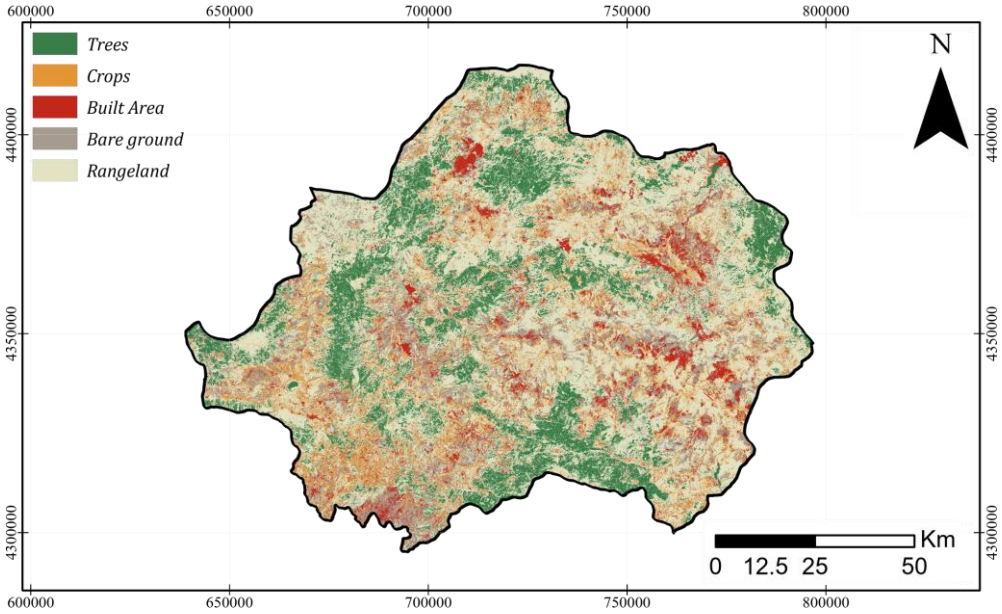

Figure 6. 2017 LULC map produced with unsupervised learning algorithms by using Landsat 8 satellite images.

In addition, the fact that these field classes cover very few surfaces in the study area is another reason. Although Landsat 8 images were resampled with a resolution of 10 meters in the pre-processing data stage, this process did not significantly improve the images' resolution. The other classes were successfully determined by unsupervised classification. Class details and the percentage of all individual classes are given in Table 4. Considering the LULC maps created for 2021 and 2017 using Landsat 8, the highest increase was seen in "Built Area" at %11.9 and "Bare Ground" at %3.2". The change in these classes are 1383.2 km2 and 376.0 km2, respectively. In addition to these, 13.9% and 2.3% decreases were calculated in "Rangeland" and "Crops" areas. The area classes and areas calculated on the LULC maps created for the years 2021 and 2017 using Sentinel-2 and Landsat 8 are given in Figure 7. "Cloud", "Flooded Vegetation", "Snow/Ice", and "Water" classes were ignored during the performance analysis of the unsupervised classifications as they cover a small area in the study area.

Table 3. 2021 and 2017 Sentinel-2 LULC maps classes.

Class	2017 (km^2)	Ratio (%)	2021 (km^2)	Ratio (%)
Bare Ground	74.2	0.6	62.3	0.5
Built Area	326.6	2.8	266.3	2.3
Crops	2005.7	17.2	1741.5	15
Flooded veg.	0.2	0	0.3	0

JSR A
Journal of Scientific Reports

Rangeland	5027.5	43.2	5464	46.9
Snow/Ice	0.2	0	0.1	0
Trees	4171.2	35.8	4069	35
Water	33.8	0.3	35.8	0.3

Table 4. 2021 and 2017 Landsat 8 LULC maps classes.

Class	2021 (km^2)	Ratio (%)	2017 (km^2)	Ratio (%)
Bare Ground	2084.4	17.9	1708.4	14.7
Built Area	2078.0	17.9	694.8	6.0
Clouds	225.6	1.9	0.0	0.0
Crops	1106.8	9.5	1380.0	11.9
Flooded veg.	0.0	0.0	0.0	0.0
Rangeland	4123.9	35.4	5744.2	49.4
Snow/Ice	0.0	0.0	0.0	0.0
Trees	2019.6	17.4	2112.1	18.1
Water	0.0	0.0	0.0	0.0

5. DISCUSSIONS and CONCLUSIONS

It is shown that the unsupervised classification was insufficient to distinguish "Clouds", "Flooded Vegetation", "Snow/Ice" and "Water" classes. The main reason for this problem is that the resolution of Landsat 8 images is smaller than the size of the areas they cover in classes where unsupervised classification is inadequate. Therefore, "Bare Ground", "Built Area", "Crops", "Rangeland" and "Trees" classes were taken into account in evaluating the performance of unsupervised classification. A similar study on the subject indicated that the Sentinel-2 may have some misleading information in water extraction, while Landsat-8 could not accurately classify urban and agricultural areas [21]. However, it is also stated that the choice of hyperparameter directly affects the output in the analyses performed with the unsupervised algorithm [22]. Considering the data obtained from the LULC maps produced for the years 2017 and 2021 unsupervised classification was insufficient to differentiate the "Bare Ground", "Built Area", "Crops" and "Trees" areas (Table 4). It is seen that unsupervised classification error in LULC maps created using Landsat 8 images, especially in the "Bare Ground", "Built Area", "Crops" and "Trees" classes, more than 2 times compared to LULC maps created using Sentinel-2 images. However, the unsupervised classification successfully defined "Rangeland" class from Landsat 8 images. Considering these reasons put forward, it is evident that maximum attention should be paid to the creation of time-series LULC maps with unsupervised classification and the analysis of land cover/land use. The use of unsupervised classification on a local scale will be inefficient due to the low resolution of Landsat 8 images, and its use in production LULC maps for larger regions will be more beneficial. At the time that unsupervised classification is preferred during the creation of LULC maps at a local scale, it is recommended to verify with high-resolution images such as Sentinel-2 and to perform class-based controls to increase the quality of final outputs.

JSR A
Journal of Scientific Reports

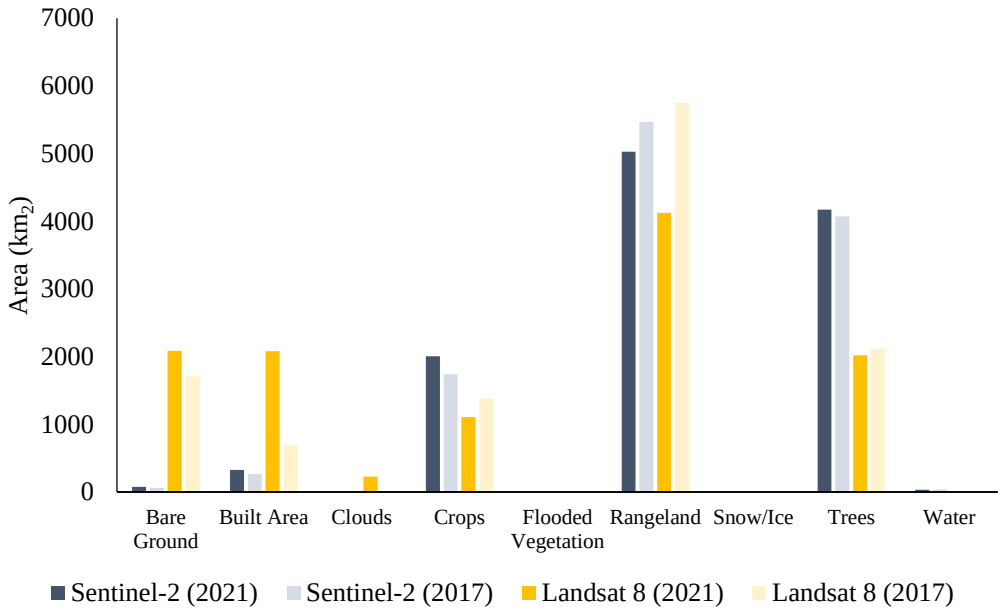

Figure 7. Distribution of Sentinel-2 and Landsat 8 based LULC maps classes.

Table 5. Distribution of cover area (km^2) Sentinel-2 and Landsat 8 based LULC maps classes.

Class	Sentinel-2 (2021)	Landsat 8 (2021)	Sentinel-2 (2017)	Landsat 8 (2017)
Bare Ground	74	2084	62	1708
Built Area	327	2078	266	695
Crops	2006	1107	1741	1380
Rangeland	5027	4124	5464	5744
Trees	4171	2020	4069	2112

This study conducted to assess the performance of unsupervised classification through high-resolution LULC maps prepared using Sentinel-2 during the production of LULC maps using Landsat 8 data. The following findings were obtained in this study;

i. Low-resolution (30 meters) LULC maps can be created by utilizing an unsupervised learning method using Landsat 8 data for large regional focus.

ii. The maximum iteration number were chosen as 50, 100 and 250 during unsupervised classification hyper-tuning processes. However, the obtained results do not reveal a significant difference when

compared with the recommended maximum number of iterations, 10-20. Therefore, the recommended values as the maximum number of iterations can be used to save computational time.
iii. The unsupervised classification algorithm was insufficient for the separation of *"Bare Ground"*, *"Built Area"*, *"Crops"* and *"Trees"* for LULC maps created by using Landsat 8 satellite.

iv. The unsupervised classification algorithm has successfully parsed fields belonging to the "Rangeland" class in both the 2017 and 2021 LULC maps.

v. It is expected that the use of supervised classification techniques to produce LULC maps by using Sentinel-2 images to compare their results with the unsupervised classification would be beneficial for future studies.

ACKNOWLEDGEMENT

The authors express their gratitude to the Kütahya Dumlupınar University for providing licensed access to ArcGIS Pro software developed by ESRI.

REFERENCES

[1] Townshend, J.R.G., (1992), Improved global data for land applications. A proposal for a new high resolution data set. Report of the Land Cover Working Group of IGBP-DIS, Global Change Report (Sweden).

[2] Duku, E., Mattah, P.A.D., and Angnuureng D.B., (2021), Assessment of land use/land cover change and morphometric parameters in the keta lagoon complex ramsar site, ghana, Water (Switzerland). 13 2537.

[3] Ekumah B., Armah, F.A., Afrifa, E.K.A., Aheto, D.W., Odoi, J.O. and Afitiri,A., (2020) Assessing land use and land cover change in coastal urban wetlands of international importance in Ghana using Intensity Analysis, Wetl Ecol Manag. 28, 271-284.

[4] Ma, Z., Liu, Z., Zhao, Y., Zhang, L., Liu, D., Ren, T., Zhang, X., and Shaoming, Li,(2020), An unsupervised crop classification method based on principal components isometric binning, ISPRS Int J Geoinf. 9(11, 648).

[5] Karra, K., Kontgis, C., Statman-Weil, Z., Mazzariello, J.C., Mathis, M., Brumby, S.P., (2021), Global land use / land cover with Sentinel 2 and deep learning, in: 2021 IEEE International Geoscience and Remote Sensing Symposium IGARSS, 4704–4707.

[6] Zanaga, D., van de Kerchove, R., de Keersmaecker, W., Souverijns, N., Brockmann, C., Quast, R., Wevers, J., Grosu, A., Paccini, A., Vergnaud, S., Cartus, O., Santoro, M., Fritz, S., Georgieva, I., Lesiv, M., Carter, S., Herold, M., Li, L., Tsendbazar, N.E., Ramoino, F., Arino, O., (2021), ESA World Cover 10 m 2020 v100.

[7] Enderle, D.I.M., Weih R.C. (2005), Integrating Supervised and Unsupervised Classification Methods to Develop a More Accurate Land Cover Classification, J Ark Acad Sci. 59, 10.

[8] Olofsson, P., Foody, G.M., Herold, M., Stehman, S.V., Woodcock, C.E., Wulder, M.A., (2014), Good practices for estimating area and assessing accuracy of land change, Remote Sens Environ. 148, 42–57.

[9] Khan, A., Hansen, M.C., Potapov, P., Adusei, B., Stehman, S.V., Steininger, M.K., (2021), An operational automated mapping algorithm for in-season estimation of wheat area for Punjab, Pakistan, 42, 3833–3849.

[10] Pickens, A.H., Hansen, M.C., Hancher, M., Stehman, S.V., Tyukavina, A., Potapov, P., Marroquin, B., Sherani, Z., (2020), Mapping and sampling to characterize global inland water dynamics from 1999 to 2018 with full Landsat time-series, Remote Sens Environ. 243, 111792.

[11] Ying, Q., Hansen, M.C., Potapov, P.V., Tyukavina, A., Wang, L., Stehman, S.V., Moore, R., Hancher, M., (2021), Global bare ground gain from 2000 to 2012 using Landsat imagery, Remote Sens Environ. 194, 161–176.

[12] Potapov, P., Li, X., Hernandez-Serna, A., Tyukavina, A., Hansen, M.C., Kommareddy, A., Pickens, A., Turubanova, S., Tang, H., Silva, C.E., Armston, J., Dubayah, R., Blair, J.B., Hofton, M., (2021), Mapping global forest canopy height through integration of GEDI and Landsat data, Remote Sens Environ. 253, 112165.

[13] Hansen, M.C., Potapov, P.V., Moore, R., Hancher, M., Turubanova, S.A., Tyukavina, A., Thau, D., Stehman, S.V., Goetz, S.J., Loveland, T.R., Kommareddy, A., Egorov, A.V., Chini, L., Justice, C.O., Townshend, J.R.G., (2013), High-resolution global maps of 21st-century forest cover change, Science. 342 (6160), 850-853.

[14] Zengin, E., A Combined Assessment of Sea Level Rise (SLR) Effect on Antalya Gulf (Türkiye) and Future Predictions on Land Loss, (2023), Journal of the Indian Society of Remote Sensing.

[15] Paris, C., Bruzzone, L., Fernandez-Prieto, D., (2019), A Novel Approach to the Unsupervised Update of Land-Cover Maps by Classification of Time Series of Multispectral Images, IEEE Transactions on Geoscience and Remote Sensing. 57, 4259–4277.

[16] Lemenkova, P., (2021), ISO Cluster classifier by ArcGIS for unsupervised classification of the Landsat TM image of Reykjavík, Bulletin of Natural Sciences Research. 11 29–37.

[17] U.S. Geological Survey 2018 Landsat collections: U.S. Geological Survey Fact Sheet, (2018), 3049.

[18] Lemenkova, P., (2021), ISO Cluster Classifier by ArcGIS for Unsupervised Classification of the Landsat TM Image of Reykjavik Iso Cluster Classifier By Arcgis For Unsupervised

Classification Of The Landsat Tm Image Of Reykjavík, Bulletin of Natural Sciences Research, 11, 29–37.

[19] Altman, N.S., (1992), An introduction to kernel and nearest-neighbor nonparametric regression, American Statistician. 46 175–185.

[20] Abburu, S., Babu Golla, S., (2015), Satellite Image Classification Methods and Techniques: A Review, Int J Comput Appl. 119 20–25.

[21] Ahady, A.B., Kaplan, G., (2022), International Journal of Engineering and Geosciences Classification comparison of Landsat-8 and Sentinel-2 data in Google Earth Engine, study case of the city of Kabul, International Journal of Engineering and Geosciences. 7, 24–31.

[22] Ghayour, L., Neshat, A., Paryani, S., Shahabi, H., Shirzadi, A., Chen, W., Al-Ansari, N., Geertsema, M., Amiri, M.P., Gholamnia, M., Dou, J., Ahmad, A., (2021), Performance evaluation of sentinel-2 and landsat 8 OLI data for land cover/use classification using a comparison between machine learning algorithms, Remote Sens (Basel), 13, 1349.